Carbon
Research

ORIGINAL ARTICLE

Open Access

Reinforcing conversion of polyselenides via a bifunctional blocking layer for efficient Li-Se batteries

Hongrui Wang[1,2,3], Qingyuan Zhao[2], Kang Lai[3], Nanyun Bao[3], Weibin Zhou[4], Qi Deng[4], Zhiqiang Fu[1], Jiayu Dai[3*], Xiongwei Wu[2*] and Xianxiang Zeng[2*]

Abstract

Lithium-selenium (Li-Se) batteries possess high volumetric capacity and have attracted considerable attention as a high energy storage system. However, the shuttling of polyselenides seriously worsens the electrochemical performance and retards their application advancement. Herein, we engineered a bifunctional membrane consisted of polyethylenimine derived carbon quantum dots (Cdots) to efficiently restrict the shuttling of polyselenides under a high Se loading (Se≈70 wt%) and promote Li-Se conversion kinetics, which can be accounted by the greatly accelerated transportation of charge carriers and dipole–dipole interactions between polar moieties and long-chain polyselenides (Li_2Se_4 and Li_2Se_6) as corroborated by theoretical calculations. Thus, the bifunctional membrane endows Li-Se batteries with a specific capacity of 658.60 mAh g^{-1} at 0.1 C and coulombic efficiency of 97.8% in average, and demonstrates the effectiveness of defect-rich Cdots on suppressing polyselenides shuttling and reinforcing Li-Se conversion kinetics in augmenting the battery's durability and efficiency.

Highlights

• A PEI-Cdots@Super P hybrid layer modified Celgrad membrane was prepared for Li-Se batteries.

• The PEI-Cdots@Super P membrane reinforces the conversion kinetics of polyselenides.

• The PEI-Cdots@Super P membrane exhibits excellent ability for restricting polyselenides.

Keywords Li-Se batteries, Carbon quantum dots, Bifunctional membrane, Polyselenides shuttle, High selenium loading

Wang *et al. Carbon Research*   (2023) 2:31

Page 2 of 9

Graphical Abstract

1 Introduction

Lithium-ion batteries (LIBs) as one of the important energy storage technologies have received great attention in the fields of mobile electronics and electronic vehicles (Chen et al. 2018; Fu and Zhong 2019; Wang et al. 2020). Nevertheless, the low energy output of LIBs is a vital barrier to the ever-increasing demand for development in the future (Luo et al. 2013; Li et al. 2019). Therefore, exploring next-generation Li-metal based energy storage systems with higher energy density is of great significance (Yang et al. 2013; Zeng et al. 2020; Chen et al. 2022). Selenium (Se), an element of the same main group as sulfur (S), has attracted extensive research interest because of its comparable electrochemical properties with S (Ding et al. 2017; Zhang et al. 2017). Moreover, the conductivity of Se is much higher than that of S, and the shuttle effect of polyselenides in carbonate-based liquid electrolytes is less serious than that of polysulfides (Liu et al. 2014; Wang et al. 2022a). Even if the higher density of Se makes the theoretical specific capacity of Li-Se batteries (675 mAh g^{-1}) inferior to that of Li–S batteries (Luo et al. 2013; Huang et al. 2019). Another merit of Li-Se batteries is the high volumetric energy density (3253 mAh cm^{-3}), making them suitable for large-scale grid energy storage and electric vehicles (Li et al. 2014; Zhang et al. 2017). Unfortunately, the Li-Se batteries still suffer from polyselenides dissolution and shuttling,

mainly (Se$_8$ → Li2Se$_x$, 4 ≤ x ≤ 8), and subsequent irreversible reactions with Li metal anode (Kim et al. 2020; Zhang et al. 2020). These problems deteriorate the cycle stability and efficiency of Li-Se batteries (Jiang et al. 2014; Yang et al. 2015).

With regard to this, numerous works focus on preparing advanced cathode materials to fundamentally eliminate polyselenide dissolution and shuttling at cathode side, including carbon host materials (Qu et al. 2015; Zeng et al. 2015) metal materials (Ma et al. 2018; Sun et al. 2021; Xia et al. 2023a) or polymer/carbon composite host as cathode materials (Kundu et al. 2013; Guo et al. 2015; Zhao et al. 2018; Zhang et al. 2019a). But many works are associated with reducing the mass loading of Se, compromising their application prospect (Zhang et al. 2020). Recently, functional membrane is another effective way to solve the shuttling problems for chalcogen-based LIBs (Ghazi et al. 2017; Wang et al. 2018; Yao et al. 2018; Xia et al. 2023b). It has been proved that the nonpolar or weakly polar materials on separator show poor inhibitory effects on polyselenide (Hou et al. 2016; Zhang et al. 2019b), which is the common choice for existing reports, but too many defects may lower the conductivity of functive on membranes (Fang et al. 2019). As a result, the ideal functive should possess adequate active sites, moderate chemical binding ability with polyselenides, and high conductivity for Li-Se conversion kinetics (Seh et al.

Wang *et al. Carbon Research*   (2023) 2:31

Page 3 of 9

2013; Chung and Manthiram 2014; Zhang et al. 2020). Zero-dimensional carbon dots (Cdots) derived from oligomer or polymer molecules are easy to disperse on substrate and help to anchor poly-sulfides/selenides without hindering the transportation of charge carriers at moderately high mass loading (Hu et al. 2019; Park et al. 2021). Polyethylenimine (PEI), as one of the typical branched polymers, possesses abundant amine groups that are beneficial for inhibiting polyselenides shuttling and Li^+ migration, if reducing its dimension to quantum dot size (Li et al. 2017; Yu et al. 2021). Hence, there is immense potential in using the PEI as precursor to synthesize Cdots for separator functionalization, and simultaneously realize the inhibition of polyselenides shuttling and acceleration of Li-Se conversion.

In this work, the PEI Cdots were blended with Super P and coated on the Celgard membrane and dried as a bifunctional layer for Li-Se batteries. Thereinto, the PEI Cdots provide abundant polar sites to restrict the shuttling of polyselenides, while Super P acts as the supporting carbon skeleton to enhance the conductivity. The electrochemical measurements proved that the bifunctional blocking layer showed excellent capability of restricting shuttle effect and accelerating charge carrier transportation for Li-Se batteries at moderately high Se loading. Furthermore, the performance of bindings and electronics in DFT calculations certified that the amino group contained in the bifunctional layer had a proper anchoring effect on long-chain polyselenides, Li_2Se_4 and Li_2Se_6, due to the distinct electronic exchange between polyselenides and the nitrogen element of PEI Cdots.

2 Materials and methods

2.1 Synthesis of PEI Cdots
The specific steps refer to the previous study (Hu et al. 2019). 1 g PEI (molecular weight=600, Aladdin) in a glass bottle was sealed with Al foil, and then carbonized under 400℃ for 50 min on a heating platform. After the glass bottle was cooled to ambient temperature, the compound was mixed with distilled water and fully dispersed with vigorous sonication for 1 h. The supernatant was acquired from the dispersion solvent after being centrifuged under 8000 r/min for 15 min, and used for dialyzing with the distilled water for 24 h. Last, the PEI Cdots were obtained after removing water by lyophilisation.

2.2 Preparation of the C/Se cathode
The preparation of C/Se composite materials followed the prior study (Wang et al. 2022b). The C/Se cathode was acquired by mixing the C/Se composite materials, Super P, SBR and CMC (weight ratio=80:10:5:5) Then, the slurry was cast onto the surface of the Al foil current collector as the C/Se cathode materials for electrochemical tests.

2.3 Preparation of PSP membrane
The PEI Cdots, Super P and PVDF (mass ratio=0.3:3:1) were mixed by mortar, dispersed in 10 mL 1-Methyl-2-pyrrolidinone (NMP) and magnetically stirred for 1 h. After the vacuum filtration step, the cast slurry was coated onto the commercial membrane for relative tests.

2.4 Electrochemical test
The CR2032-type Li-Se batteries were assembled using the C/Se composite materials as the cathode, lithium foil as the anode, Celgard membrane or PSP membrane as the interlayer between the cathode and anode, and 1 M $LiPF_6$ as electrolyte. The charge–discharge measurements of Li-Se batteries were conducted using the LAND CT2001A. The EIS tests were completed on the electrochemical workstation CHI 760d (Chenhua, Shanghai).

2.5 Materials characterizations
Scanning electron microscopy (SEM) and elemental mapping images were taken by using a JEOL JSM-6701F. The FTIR of PSP and Super P were characterized by a Bruker Alpha which ranged from $3500 \sim 1000$ cm^{-1}. The XPS analyses were performed using the Thermo Scientific K-Alpha. The XRD measurements were carried out via the SHIMADZU with the range set to 10–80° and a Cu Kα as the radiation. The TGA analysis was carried out via the METTLER under the argon atmosphere.

2.6 Computational details
All the geometry structure relaxations for first principles calculations were carried out within the density functional theory through Vienna Ab Simulation Package (VASP) (Hohenberg and Kohn 1964; Kresse and Furthmüller 1996). The Perdew-Burke-Ernzerhof type was used to represent the exchange–correlation function. The electron–ion interactions between the constituent atoms were described through the projector augmented wave (PAW) method (Hou et al. 2016). The Van Der Waals interactions between substrate materials surface and Li_2Se_n ($n=4$ and 6) were considered using the optPBE-vdW functional. The energy cut off was set to 500 eV for all the calculations in this work. The convergence criterions of energy and force calculations had been achieved with 10^{-5} convergence and 0.02 eV $\mathring{A}^{-1}$, respectively. The Brillouin zone sampling was set to the Gamma-centered grids with a k-point mesh $3 \times 3 \times 1$. The density of states (DOS) was also analyzed with the k-points mesh $11 \times 11 \times 1$ in the Gamma-centered grids. The vacuum layer of 15 Å was used to avoid the interactions of adjacent configurations.
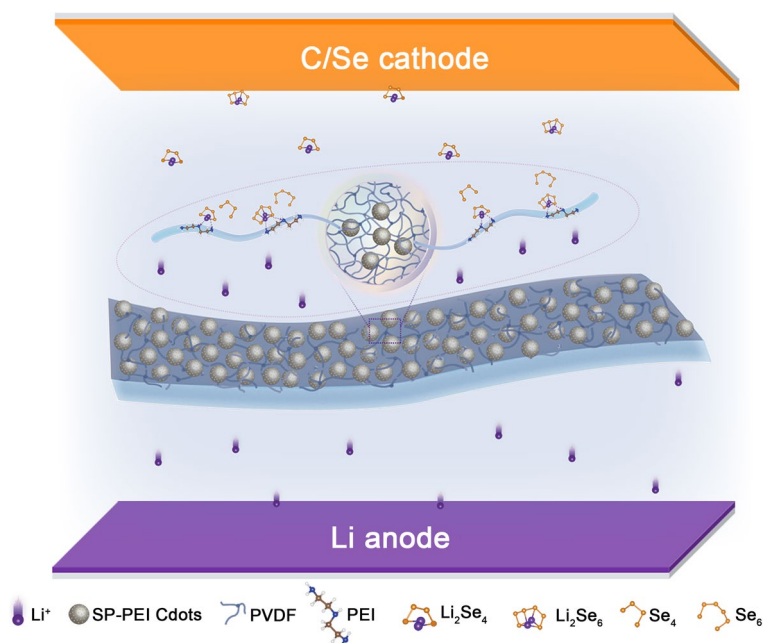
Fig. 1 Schematic of the PSP membrane and confine mechanism for Li_2Se_n
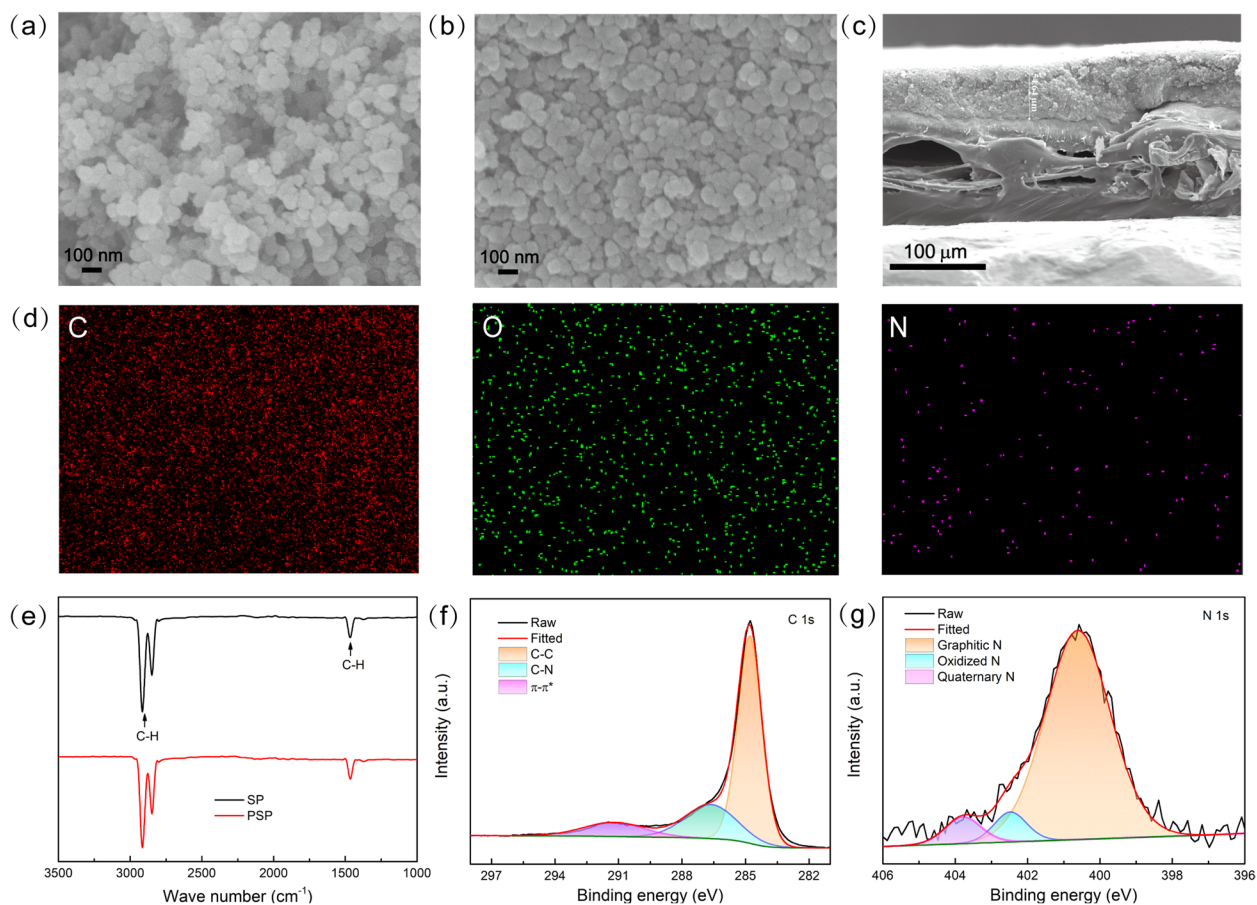

Fig. 2 SEM images of (**a**) SP and (**b**) PSP membranes. (**c**) The cross-section of the PSP membranes. **d** Corresponding EDX elemental mapping images. **e** The FTIR spectra comparison between the SP and PSP membranes. **f** The C1s and (**g**) N1s XPS spectra of PSP membrane

Wang *et al. Carbon Research*   (2023) 2:31

Page 5 of 9

Herein, the binding energy (E_b) was on this equation: $E_b = E_{polyselenide} + E_{substrate} - E_{(polyselenide-substrate)}$, where $E_{polyselenide}$, $E_{substrate}$ and $E_{(polyselenide-substrate)}$ represent the energy of different individual polyselenides (Li_2Se_n, $n = 4$ and 6), the energy of the isolated different substrate surfaces and the total energy of the Li_2Se_n binding on different substrates.

3 Results

The PEI Cdots were carbonized by a "one-pot" method, which is a facile method for the synthesis of Cdots. Specifically, PEI Cdots were developed by being carbonized, which served as the source of the surface functional group. After that, the PEI Cdots were blended with Super P and polyvinylidene fluoride (PVDF) to form a suspension and filtered onto the Celgard separator to obtain the target membrane (PSP) (Fig. 1). During the discharge process, the polyselenides were confined within cathode side by PSP, reducing the capacity loss caused by the shuttle effect under the high Se mass loading. For comparision, the Super P and PVDF were employed to form a suspension and filtered onto the Celgard separator to obtain the SP membrane.

To observe the morphology and structure characteristics of the SP and PSP membrane, SEM characterizations were carried out. As shown in Fig. 2a-c, the Super
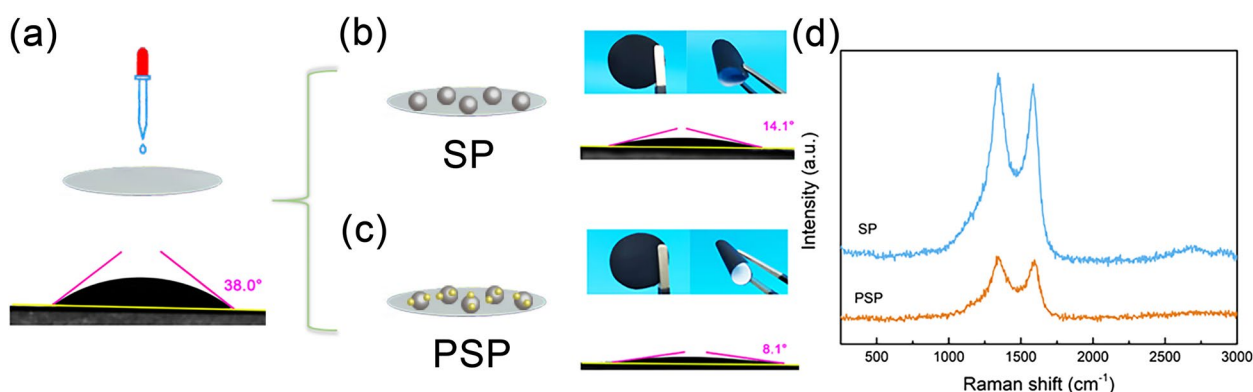

Fig. 3 Schematic and contact angle images of (**a**) Celgard, (**b**) SP and (**c**) PSP membranes with electrolytes (top sets are their digital images). **d** Raman spectra of SP and PSP membranes
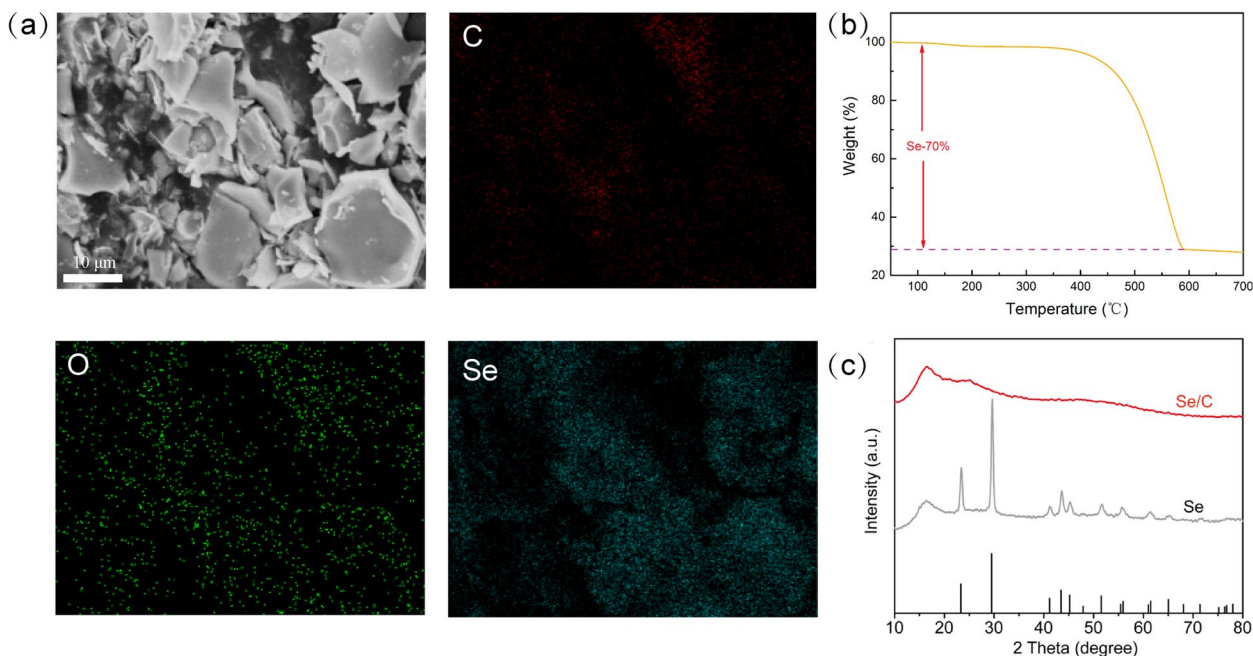

Fig. 4 **a** SEM images and of EDS elemental mapping of C/Se composite materials. **b** TGA curves of C/Se. **c** XRD patterns of C/Se, Se powder and PDF standard card of Se (PDF#06–0362)

P, as an interconnected porous skeleton, lays the foundation for the composite, which facilitates the migration of selenium ions in it, while the PEI Cdots decorate on it after filtration, and forms a conformal porous coating on the Clegard separator. Its porosity shortens the length of ion diffusion and provides a large specific surface area to facilitate the redox reaction between Se and Li^+ at cathode. At the same time, the polar groups on the PEI Cdots are beneficial to restrict the shuttle effect. The EDS element mappings also confirm the uniform element distribution of PSP on the Celgard separator surface (Fig. 2d).

To explore the bonds in the composite, the structure of the as-prepared PSP membrane was further investigated by Fourier transform infrared spectroscopy (FTIR) spectra. As shown in Fig. 2e, only the C-H stretching adsorption sites were observed at 2900–2700 cm^{-1} and 1460 cm^{-1} from the FTIR spectra of both SP and PSP membranes. The characteristic spectrums of amine did not appear because the content of N element in PSP was low (Boronat et al. 2009; Wepasnick et al. 2011). But from the results from X-ray photoelectron spectroscopy (XPS) of PSP, three peaks could be observed in the unrolled integration signals of C1s, corresponding to the combination of C–C binding (284.8 eV), C-N amine bonding (286.7 eV), and π-π* (291.3 eV), respectively (Fig. 2f) (Chen et al. 2020). Meanwhile, the signals of N 1 s can be observed in Fig. 2g, corresponding to the combination of graphitic

N (400.6 eV), oxidized N (402.4 eV), and quaternary N (403.7 eV), respectively (Hellgren et al. 2016; Hu et al. 2019). The above results indicated that the PEI Cdots were preserved in the PSP membrane, which acted as the functional source of nitrogen and oxygen.

The high wettability of PSP membrane to electrolyte could reflect its low impedance toward mass transportation, which also contributes to low membrane resistance for charge transfer. As shown in Fig. 3a-c, the contact angles of Celgard, SP and PSP membrane were 38.0, 14.1 and 8.1, respectively. Due to the introduction of polar groups, the PSP showed the smallest contact angle than other two separators. Meanwhile, according to the Raman spectra of SP and PSP, the peaks of the defected and disordered carbon were detected at ~1350 cm^{-1} and the peaks of the sp^2 hybrid carbon were shown at ~1580 cm^{-1} (Fig. 3d). In addition, the peak intensity of I_D/I_G in PSP (about 1.00) was almost the same with SP (1.01), signifying the excellent electric conductivity of PSP.

To check the efficacy of PSP membrane, a high-loading C/Se cathode was prepared. As shown in Fig. 4a, there was no distinct bulky Se existing on the surface of carbon materials, and the Se and C, O elements distribute homogeneously in the C/Se composites. The mass loading of Se in the C/Se composite was measured to be 70% using thermogravimetric analysis (TGA, Fig. 4b). As shown in X-ray diffraction (XRD) patterns, the diffraction peaks of the crystalline phase Se in C/Se disappeared (Fig. 4c), it means Se element in the carbon host is amorphous.
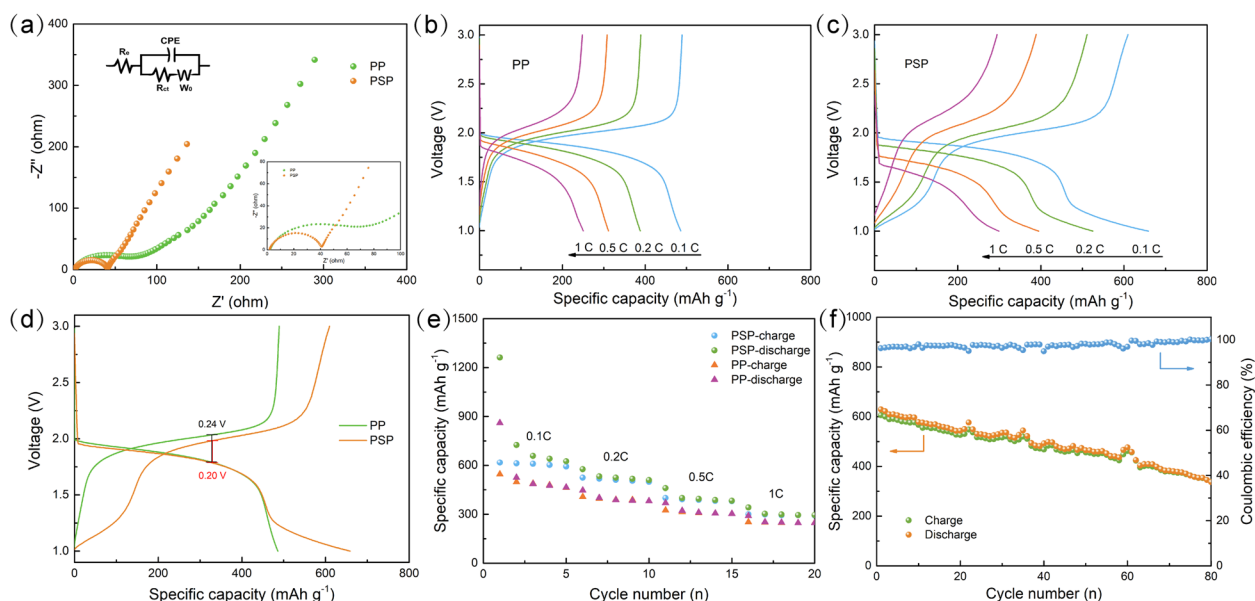

Fig. 5 (**a**) The electrochemical impedance spectra (EIS) of the Li-Se batteries with different PP and PSP membranes before cycling (the inset is the magnified image for the Li-Se batteries with PP or PSP membrane). Rate performance with PP (**b**) and PSP (**c**) membrane for Li-Se batteries. (**d**) The second cycle performance comparison plots at 0.1 C with various membranes. (**e**) Cycling performance at different rates. (**f**) The long-term cycling stability performance of Li-Se batteries with PSP membrane at 0.05 C

Then, the Li-Se batteries were prepared with the C/Se composite materials cathode, the metal lithium anode, and the pure Celgard (PP) separator or PSP membrane. Comparison of interfacial charge transfer capability between various membranes was conducted via electrochemical impedance spectroscopy (EIS). As shown in Fig. 5a, there is a single semicircle in the high frequency region of two kinds of battery. According to the equivalent circuit, Ohmic resistance of the ingredient for electrolyte and battery (R_e), charge transfer resistance of the electrode reaction kinetics (R_{ct}), the constant phase element (CPE), and the Warburg impedance (W_0) are involved (Fang et al. 2015). The resistance of Li-Se batteries with PSP membrane (41.20 Ω) was lower than that using PP membrane (70.03 Ω), because PSP serves as the interconnected porous skeleton and endows the Celgard separator substrate with high electronic conductivity (Su and Manthiram 2012). The rate performance

from the third cycle of PP and PSP membrane for Li-Se batteries was further explored with the rate from 0.1 C to 1 C (Fig. 5b-c). Different from the rapidly decreased capacity of the PP membrane (from 485.99 mAh g^{-1} at 0.1 C to 250.26 mAh g^{-1} at 1 C), the PSP membrane exhibited a superior rate capability at 0.1 C (658.60 mAh g^{-1}) and maintained approximately 300 mAh g^{-1} when the rate was increased to 1 C. Furthermore, the voltage polarization difference of the PSP membrane (0.20 V) was smaller than that of the PP membranes (0.24 V) (Fig. 5d). More interesting, the Li-Se batteries with the PSP membrane exhibited an apparent enhancement in specific capacity, which was resulted from further conversion of polyselenides (Li$_2$Se$_2$ → Li$_2$Se) at the discharge plateau of approximately 1.2 V (Lei et al. 2022). Such different charge–discharge behaviour indicates that the introduction of PEI Cdots, we think, reinforces the Li-Se conversion kinetics. The cycling performance of PP and PSP
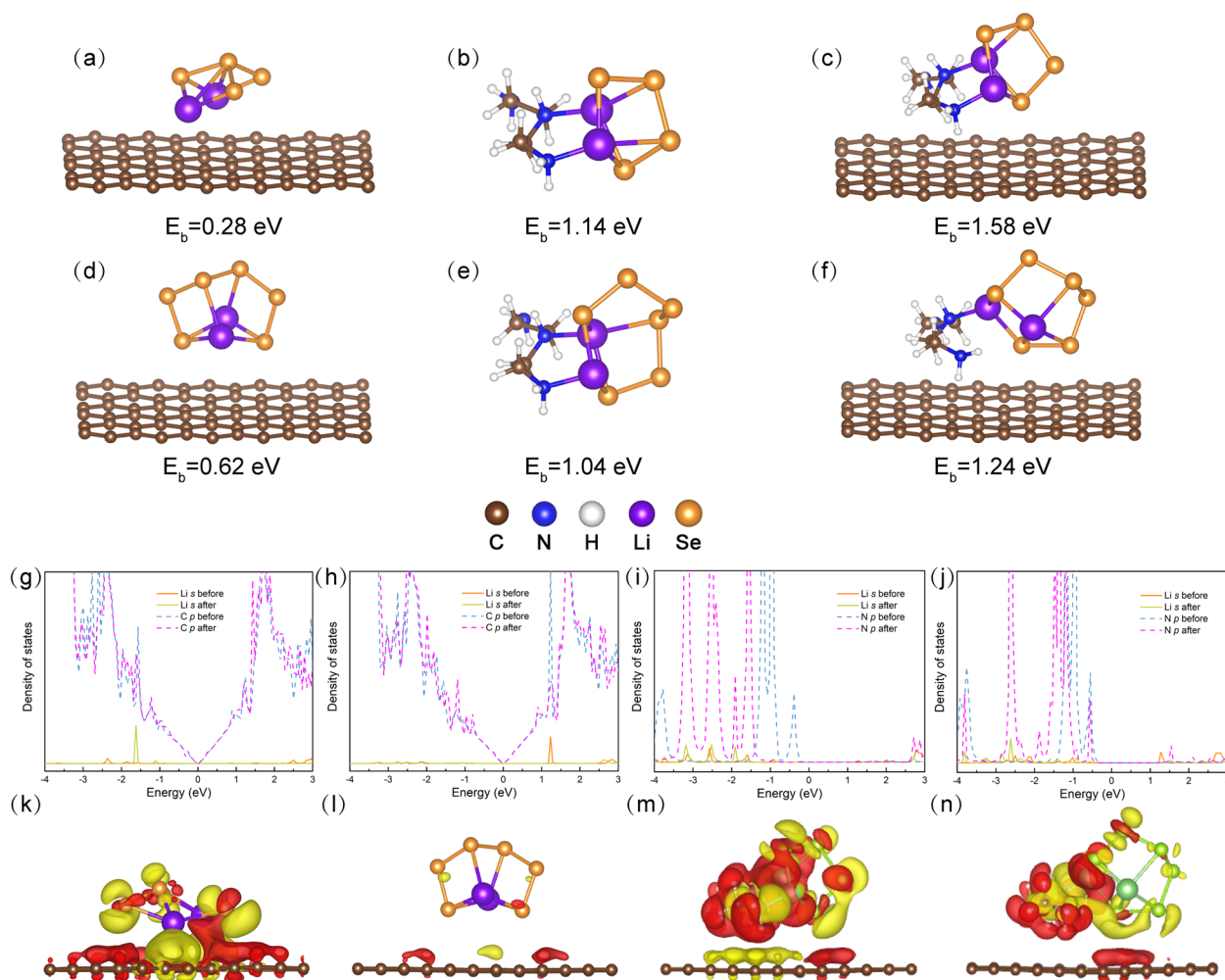

Fig. 6 Optimized molecular models of the interactions of Li$_2$Se$_4$ and Li$_2$Se$_6$ binding on Super P (**a**, **b**), PEI Cdots (**c**, **d**), and PSP (**e**, **f**) substrate materials along with the corresponding binding energies. Partial density of states (PDOS) of Li$_2$Se$_4$ binding on SP (**g**) and PSP (**i**) membrane and the Li$_2$Se$_6$ binding on SP (**h**) and PSP (**j**) membrane before and after the interaction. Electron density differences of Li$_2$Se$_4$ binding on SP (**k**) and PSP (**m**) membrane and the Li$_2$Se$_6$ binding on SP (l) and PSP (**n**) membrane

Wang *et al. Carbon Research*   (2023) 2:31

Page 8 of 9

membranes at various rates are exhibited in Fig. 5e. Different from the rapidly deteriorated specific capacity of the PP-based Li-Se batteries, the PSP membrane enables Li-Se batteries to exhibit superior specific capacities of 1262.00 mAh g^{-1} at 0.1 C and then become at 658.60 mAh g^{-1}, and 341.60 mAh g^{-1} at 1 C, which is attributed to the enhancement of interfacial kinetics with the introduction of the PEI-Cdots and Super P. Additionally, the Li-Se batteries with PSP can still maintain a reversible capacity of 330.50 mAh g^{-1} after 80 cycles at 0.05 C and an average coulombic efficiency of 97.78% after rate test (Fig. 5f), which displays better electrochemical performance than that of PP.

Results mentioned above were further confirmed by the calculations from electronic performance. Different from the SP, the significant energy shifts can be observed from the partial density of states (PDOS) of PSP and Li$_2$Se$_n$ ($n = 4$, 6), before and after the binding, as shown in Fig. 6g-j. In the PDOS plots, the energy downshift of the PSP substrate and the energy upshift of Li$_2$Se$_n$ can be observed during the binding, which signifies that PSP can cause charge exchange and polar-polar interaction with Li$_2$Se$_n$. The electron charge density differences in Li$_2$Se$_n$ adsorbed on PSP are illustrated in Fig. 6k-n. The yellow and red areas represent the accumulation and depletion of charges. Compared with SP, there is a larger charge accumulation area in PSP, which contributes to the effective prohibition of polyselenides shuttling.

4 Conclusions

In conclusion, we have proposed a bifunctional blocking layer that acts as an effective barrier for Li-Se batteries to inhibit the shuttle effect of polyselenides under a selenium loading of 70 wt%. The EIS and DFT calculations confirm that the PSP can increase the conductivity and greatly promote the migration of electrons and ions, accelerating the interfacial charge transfer and maintaining a stable releasing capacity and over 97% Coulombic efficiency at low rate, when side reactions are attenuated. Besides, it is found that the PEI Cdots provides additional active sites for promoted Li-Se conversion kinetics. This study provides a facile but efficient membrane engineering strategy for efficiently inhibiting redox species shuttling and reinforcing conversion at moderately high mass loading, promoting the advancement of energy-dense metal batteries.

Supplementary Information

The online version contains supplementary material available at https://doi.org/10.1007/s44246-023-00064-2.

Additional file 1: Fig. S1. Partial density of states (PDOS) of Li$_2$Se$_4$ (a, b) and Li$_2$Se$_6$ (c, d) adsorption on SP separator before and after the interaction. **Fig. S2.** Electron density differences of Li$_2$Se$_4$ (a) and Li$_2$Se$_6$ (b) adsorption on PSP separator. **Fig. S3.** Thermogravimetric analysis curves of C/Se.

Author's contributions
Conceptualization and Funding acquisition: Xianxiang Zeng, Xiongwei Wu, and Jiayu Dai; Investigation and Methodology: H.-R. Wang; Writing-original draft: Hongrui Wang and Qingyuan Zhao; Formal Analysis: Kang Lai, Nanyun Bao, and Zhiqiang Fu; Resources and Software: Jiayu Dai; Writing-review & editing: Xianxiang Zeng, Weibin Zhou and Qi Deng. All authors read and approved the final manuscript.

Availability of data and materials
The datasets used or analyzed during the current study are available from the corresponding author on reasonable request.

Declarations

Competing interests
All authors declare that there are no competing interests.

Author details
[1]College of Agronomy, Hunan Agricultural University, Changsha 410128, People's Republic of China. [2]School of Chemistry and Materials Science, Hunan Agricultural University, Changsha 410128, People's Republic of China. [3]Hunan Key Laboratory of Extreme Matter and Applications, National University of Defense Technology, Changsha 410073, China. [4]State Key Laboratory of Utilization of Woody Oil Resource of China, Hunan Provincial Key Laboratory of Oils and Fats Molecular Structure and Function, Hunan Academy of Forestry, Changsha 410128, People's Republic of China.

References

Boronat M, Concepción P, Corma A (2009) Unravelling the nature of gold surface sites by combining IR spectroscopy and DFT calculations. Implications in catalysis. J Phys Chem C 113:16772–16784

Chen W, Lei T, Qian T, Lv W, He W, Wu C, Liu X, Liu J, Chen B, Yan C, Xiong J (2018) A New Hydrophilic Binder Enabling Strongly Anchoring Polysulfides for High-Performance Sulfur Electrodes in Lithium-Sulfur Battery. Adv Energy Mater 8:1702889

Chen X, Wang X, Fang D (2020) A review on C1s XPS-spectra for some kinds of carbon materials. Fuller Nanotub Carbon Nanostruct 28:1048–1058

Chen Z, Chang Z, Liu Z, Zhou N (2022) Functionalized M$_2$CT$_2$ (M= Ti, V, Cr, Mn; T= O, S, Se) MXenes as anchoring materials for lithium-sulfur batteries. Appl Surf Sci 602:154375

Chung SH, Manthiram A (2014) Bifunctional separator with a light-weight carbon-coating for dynamically and statically stable lithium-sulfur batteries. Adv Funct Mater 24:5299–5306

Ding J, Zhou H, Zhang H, Tong L, Mitlin D (2017) Selenium Impregnated Monolithic Carbons as Free-Standing Cathodes for High Volumetric Energy Lithium and Sodium Metal Batteries. Adv Energy Mater 8:1701918

Wang *et al. Carbon Research*   (2023) 2:31

Page 9 of 9

Fang R, Zhou G, Pei S, Li F, Cheng HM (2015) Localized polyselenides in a graphene-coated polymer separator for high rate and ultralong life lithium-selenium batteries. Chem Commun 51:3667–3670

Fang D, Wang Y, Liu X, Yu J, Qian C, Chen S, Wang X, Zhang S (2019) Spider-Web-Inspired Nanocomposite-Modified Separator: Structural and Chemical Cooperativity Inhibiting the Shuttle Effect in Li-S Batteries. ACS Nano 13:1563–1573

Fu X, Zhong W-H (2019) Biomaterials for High-Energy Lithium-Based Batteries: Strategies, Challenges, and Perspectives. Adv Energy Mater 9:1901774

Ghazi ZA, He X, Khattak AM, Khan NA, Liang B, Iqbal A, Wang J, Sin H, Li L, Tang Z (2017) MoS2/celgard separator as efficient polysulfide barrier for long-life lithium-sulfur batteries. Adv Mater 29:1606817

Guo J, Wen Z, Ma G, Jin J, Wang W, Liu Y (2015) A selenium@polypyrrole hollow sphere cathode for rechargeable lithium batteries. RSC Adv 5:20346–20350

Hellgren N, Haasch RT, Schmidt S, Hultman L, Petrov I (2016) Interpretation of X-ray photoelectron spectra of carbon-nitride thin films: New insights from in situ XPS. Carbon 108:242–252

Hohenberg P, Kohn W (1964) Inhomogeneous Electron Gas. Phys Rev 136:B864

Hou T, Chen X, Peng H-J, Huang J, Li B-Q, Zhang Q, Li B (2016) Design Principles for Heteroatom-Doped Nanocarbon to Achieve Strong Anchoring of Polysulfides for Lithium-Sulfur Batteries. Small 12:3283–3291

Hu Y, Chen W, Lei T, Zhou B, Jiao Y, Yan Y, Du X, Huang J, Wu C, Wang X, Wang Y, Chen B, Xu J, Wang C, Xiong J (2019) Carbon Quantum Dots-Modified Interfacial Interactions and Ion Conductivity for Enhanced High Current Density Performance in Lithium-Sulfur Batteries. Adv Energy Mater 9:1802955

Huang X, Wang W, Deng J, Gao W, Liu D, Ma Q, Xu M (2019) A Se-hollow porous carbon composite for high-performance rechargeable K-Se batteries. Inorg Chem Front 6:2118–2125

Jiang S, Zhang Z, Lai Y, Qu Y, Wang X, Li J (2014) Selenium encapsulated into 3D interconnected hierarchical porous carbon aerogels for lithium-selenium batteries with high rate performance and cycling stability. J Power Sources 267:394–404

Kim S, Cho M, Lee Y (2020) High-Performance Li-Se Battery Enabled via a One-Piece Cathode Design. Adv Energy Mater 10:1903477

Kresse G, Furthmüller J (1996) Efficient Iterative Schemes for Ab Initio Total-Energy Calculations Using a Plane-Wave Basis Set. Phys Rev B 54:11169

Kundu D, Krumeich F, Nesper R (2013) Investigation of nano-fibrous selenium and its polypyrrole and graphene composite as cathode material for rechargeable Li-batteries. J Power Sources 236:112–117

Lei Y, Liang X, Yang L, Chen J, Qu L, Xu K, Feng J (2022) Li-Se batteries: Insights to the confined structure of selenium in hierarchical porous carbon and discharge mechanism in the carbonate electrolyte. Carbon 191:122–131

Li Z, Yuan L, Yi Z, Liu Y, Huang Y (2014) Confined selenium within porous carbon nanospheres as cathode for advanced Li-Se batteries. Nano Energy 9:229–236

Li Y, Fan J, Zhang J, Yang J, Yuan R, Chang J, Zheng M, Dong Q (2017) A honeycomb-like Co@N-C composite for ultrahigh sulfur loading Li-S batteries. ACS Nano 11:11417–11424

Li J, Chen C, Chen Y, Li Z, Xie W, Zhang X, Shao M, Wei M (2019) Polysulfide Confinement and Highly Efficient Conversion on Hierarchical Mesoporous Carbon Nanosheets for Li-S Batteries. Adv Energy Mater 9:1901935

Liu Y, Si L, Zhou X, Liu X, Xu Y, Bao J, Dai Z (2014) A selenium-confined microporous carbon cathode for ultrastable lithium-selenium batteries. J Mater Chem A 2:17735–17739

Luo C, Xu Y, Zhu Y, Liu Y, Zheng S, Liu Y, Langrock A, Wang C (2013) Selenium@Mesoporous Carbon Composite with Superior Lithium and Sodium Storage Capacity. ACS Nano 7:8003–8010

Ma D, Li Y, Yang J, Mi H, Luo S, Deng L, Yan C, Zhang P, Lin Z, Ren X, Li J, Zhang H (2018) Atomic layer deposition-enabled ultrastable freestanding carbon-selenium cathodes with high mass loading for sodium-selenium battery. Nano Energy 43:317–325

Park J, Moon J, Ri V, Lee S, Kim C, Cairns EJ (2021) Nitrogen-Doped Graphene Quantum Dots: Sulfiphilic Additives for the High-Performance Li-S Cells. ACS Appl Energ Mater 4:3518–3525

Qu Y, Zhang Z, Zhang X, Ren G, Lai Y, Liu Y, Li J (2015) Highly ordered nitrogen-rich mesoporous carbon derived from biomass waste for high-performance lithium-sulfur batteries. Carbon 84:399–408

Seh ZW, Li W, Cha JJ, Zheng G, Yang Y, McDowell MT, Hsu P-C, Cui Y (2013) Sulphur-TiO2 yolk-shell nanoarchitecture with internal void space for long-cycle lithium-sulphur batteries. Nat Commun 4:1–6

Su Y-S, Manthiram A (2012) Lithium-sulphur batteries with a microporous carbon paper as a bifunctional interlayer. Nat Commun 3:1–6

Sun T, Zhao X, Li B, Shu H, Luo L, Xia W, Chen M, Zeng P, Yang X, Gao P (2021) NiMoO4 Nanosheets Anchored on N-S Doped Carbon Clothes with Hierarchical Structure as a Bidirectional Catalyst toward Accelerating Polysulfides Conversion for Li-S Battery. Adv Funct Mater 31:2101285

Wang H, Jiang Y, Manthiram A (2018) Long Cycle Life, Low Self-Discharge Sodium-Selenium Batteries with High Selenium Loading and Suppressed Polyselenide Shuttling. Adv Energy Mater 8:1701953

Wang R, Yang J, Chen X, Zhao Y, Zhao W, Qian G, Li S, Xiao Y, Chen H, Ye Y, Zhou G, Pan F (2020) Highly Dispersed Cobalt Clusters in Nitrogen-Doped Porous Carbon Enable Multiple Effects for High-Performance Li-S Battery. Adv Energy Mater 10:1903550

Wang C-Y, Dong W-D, Wang L, Wu L, Hu Z-Y, Chen L-H, Li Y, Su B-L (2022a) Dual Catalysis-adsorption Function Modified Separator Towards High-Performance Li-Se Battery. Appl Surf Sci 599:153932

Wang H, Lai K, Guo F, Long B, Zeng X, Fu Z, Wu X, Xiao Y, Dou S, Dai J (2022b) Theoretical calculation guided materials design and capture mechanism for Zn-Se batteries via heteroatom-doped carbon. Carbon Neutral 1:59–67

Wepasnick KA, Smith BA, Schrote KE, Wilson HK, Diegelmann SR, Fairbrother DH (2011) Surface and structural characterization of multi-walled carbon nanotubes following different oxidative treatments. Carbon 49:24–36

Xia W, Han M, Chen Y, Zhou Y, Shu H, Chen Y, Su J, Wang X (2023b) NiFeP Anchored on rGO as a Multifunctional Interlayer To Promote the Redox Kinetics for Li-S Batteries via Regulating d-Bands of Ni-Based Phosphides. ACS Sustain Chem Eng 11:1742–1751

Xia W, Chen Y, Wang W, Lu Y, Chen Y, Chen M, Yang X, Gao P, Shu H, Wang X (2023aa) Enhanced catalytic activity of Co-CoO via VC$_{0.75}$ heterostructure enables fast redox kinetics of polysulfides in Lithium-Sulfur batteries. Chem. Eng. J 458:141477

Yang CP, Xin S, Yin YX, Ye H, Zhang J, Guo YG (2013) An advanced selenium-carbon cathode for rechargeable lithium-selenium batteries. Angew Chem Int Edit 52:8363–8367

Yang C-P, Yin Y-X, Guo Y-G (2015) Elemental selenium for electrochemical energy storage. J Phys Chem Lett 6:256–266

Yao S, Cui J, Huang JQ, Lu Z, Deng Y, Chong WG, Wu J, Haq IU, M., Ciucci, F., Kim, J.K., (2018) Novel 2D Sb$_2$S$_3$ nanosheet/CNT coupling layer for exceptional polysulfide recycling performance. Adv Energy Mater 8:1800710

Yu B, Huang A, Srinivas K, Zhang X, Ma F, Wang X, Chen D, Wang B, Zhang W, Wang Z, He J, Chen Y (2021) Outstanding catalytic effects of 1T'-MoTe$_2$ quantum dots@3D graphene in shuttle-free Li-S batteries. ACS Nano 15:13279–13288

Zeng L, Zeng W, Jiang Y, Wei X, Li W, Yang C, Zhu Y, Yu Y (2015) A flexible porous carbon nanofibers-selenium cathode with superior electrochemical performance for both Li-Se and Na-Se batteries. Adv Energy Mater 5:1401377

Zeng X-X, Chen H, Guo G, Li S-Y, Liu J-Y, Ma Q, Liu G, Yin Y-X, Wu X-W, Guo Y-G (2020) Raising the capacity of lithium vanadium phosphate via anion and cation co-substitution. Sci China Chem 63:203–207

Zhang S-F, Wang W-P, Xin S, Ye H, Yin Y-X, Guo Y-G (2017) Graphitic Nanocarbon-Selenium Cathode with Favorable Rate Capability for Li-Se Batteries. ACS Appl Mater Interfaces 9:8759–8765

Zhang F, Xiong P, Guo X, Zhang J, Yang W, Wu W, Liu H, Wang G (2019a) A nitrogen, sulphur dual-doped hierarchical porous carbon with interconnected conductive polyaniline coating for high-performance sodium-selenium batteries. Energy Storage Mater 19:251–260

Zhang T, Wang H, Zhao J (2019b) Heterostructures of doped graphene and MoX$_2$ (X = S and Se) as promising anchoring materials for lithium-sulfur batteries: a first-principles study. New J Chem 43:9396–9402

Zhang F, Guo X, Xiong P, Zhang J, Song J, Yan K, Gao X, Liu H, Wang G (2020) Interface Engineering of MXene Composite Separator for High-Performance Li-Se and Na-Se Batteries. Adv Energy Mater 10:2000446

Zhao X, Yin L, Zhang T, Zhang M, Fang Z, Wang C, Wei Y, Chen G, Zhang D, Sun Z, Li F (2018) Heteroatoms dual-doped hierarchical porous carbon-selenium composite for durable Li-Se and Na-Se batteries. Nano Energy 49:137–146

Publisher's Note